Pergamon

Cement and Concrete Research 29 (1999) 1225–1238

CEMENT AND CONCRETE RESEARCH

Characterization and identification of equilibrium and transfer moisture properties for ordinary and high-performance cementitious materials

V. Baroghel-Bouny[a,*], M. Mainguy[a], T. Lassabatere[b], O. Coussy[a]

[a]*Laboratoire Central des Ponts et Chaussées, 58 Bd Lefebvre, F-75732 Paris Cedex 15, France*
[b]*Commissariat à l'Energie Atomique, F-91191 Gif sur Yvette, France*

Received 27 July 1998; accepted 10 May 1999

Abstract

In this paper some aspects of equilibrium and transfer moisture properties of high-performance materials are presented and compared with ordinary cement pastes and concretes. First, the equilibrium moisture properties of the hardened materials are described by means of water vapour sorption isotherms, which illustrate the hysteretical behaviour of the materials. Experimental results of drying shrinkage versus relative humidity (RH) are also reported here. These experimental data are in good agreement with the numerical results provided by a thermodynamic modelling based on capillary stresses and hygromechanical couplings. In particular the linearity of the strains-RH curve over a wide range is pointed out in both cases. Isothermal drying process at RH = 50% has experimentally and numerically been studied. After identification of the intrinsic permeability of the materials from experimental weight losses, numerical moisture profiles were compared with gamma-ray attenuation measurements. The influence of the initial moisture state of the materials that results from self-desiccation in particular was pointed out on the evolution of the moisture profiles as a function of time.

Keywords: Drying; Humidity; Permeability; Shrinkage; High-performance concrete

1. Introduction

In recent years, durability of cement-based materials has becoming a key topic. Since these materials are porous, their durability is basically determined by their ability to resist the penetration of aggressive agents. Furthermore, since every degradation mechanism involves water, the knowledge of the moisture properties of the material is of prime interest.

Moisture transfers occur during the whole lifetime of concrete structures. In the simplest case, they occur through the drying process of the material, when it is submitted to a lower environmental relative humidity than its internal one. This phenomenon affects the surface zone of many civil engineering structures. Moreover, these processes are also often combined with other mass transport processes or with chemical reactions that occur in nonsaturated conditions, such as carbonation or penetration of chloride ions. All of these facts point out the basic need to understand perfectly and to be able to forecast moisture transfers and the drying process in particular.

A change of the moisture state of the material induces not only mass transfer, but also deformations. These deformations, when restrained, can lead to damage and severe cracking of the structure.

In addition to contributing to a better understanding of the characterization of equilibrium and transfer moisture properties, a particular aim of the study presented in this paper was to highlight the similarities and the differences between the behaviour of high-performance materials and ordinary materials.

2. Materials

In the research reported in this paper, two cement pastes, CO and CH, and two concretes, BO and BH, were studied. The mix compositions of the different materials are given in Table 1. The mixes CO and BO correspond to ordinary materials, while CH and BH, which were mixed with a low water-to-cement ratio (W/C) and which contain silica fume (SF) and superplasticizer (SP), are high-performance (HP) materials. The materials were prepared with a type I normal Portland cement. The mineral composition of this cement, calculated by Bogue's formula from the chemical composition, is given in Table 2. This cement is rich in C_3S

* Corresponding author. Tel.: +33-14-043-5132; fax: +33-14-043-5498.
E-mail address: baroghel@lcpc.fr (V. Baroghel-Bouny)

0008-8846/99/$ – see front matter
PII: S0008-8846(99)00102-7

Table 1
Composition of mixes (mass proportions)

Mix	W/C	Additives	Aggregate/C	Sand/gravel
CO	0.34	–	–	–
CH	0.19	SF/C = 0.10 and SP/C = 0.018	–	–
BO	0.48	–	5.48	0.62
BH	0.26	SF/C = 0.10 and SP/C = 0.018	4.55	0.51

(57.28%), inducing high strength at early age. It has a low C_3A content (3.03%) inducing low water demand, which gives a good workability despite the low W/C of the HP materials. The Blaine fineness of the cement is 342 $m^2 \cdot kg^{-1}$. The silica fume is added as dry powder. Its SiO_2 content is 87% and its Brunauer, Emmet, Teller (BET) specific surface area (measured by nitrogen adsorption) is 17.6 $m^2 \cdot g^{-1}$. The superplasticizer is a formaldehyde-naphthalene sulfonate copolymer. The concretes are prepared with limestone aggregates (maximum size, 20 mm).

The 28-day compressive strength of the HP concrete BH is 115.5 MPa. For the ordinary concrete BO, the value is 49.4 MPa.

3. Internal relative humidity

The internal relative humidity of a material is the relative humidity (RH) of the gaseous phase in equilibrium with the interstitial liquid phase in the pore network of the material.

Cement hydration processes consume water molecules. This induces a liquid water content decrease in cementitious materials while the microstructure is hardening and the pore structure is refining. There is development of gas/liquid menisci in the pore network and depression in the pore water. From a given degree of hydration of the cement and depending on the initial water content, more generally on the mix-parameters, the material exhibits self-desiccation (internal drying). This means that the material undergoes a decrease of its internal RH while hardening, when it is not in contact with an external moisture source. Furthermore, it can be noticed that, in the case of HP materials (mixed with SF), as a result of their compactness, the core of samples can undergo self-desiccation even if the samples are under wet external conditions [1,2].

The internal RH decrease can be measured continuously in laboratory on hydrating samples protected from moisture exchange with the surroundings and stored at constant temperature (method first applied by Copeland and Bragg [3]). Here, the measurement is made with samples immediately enclosed into sealed cells upon casting. Each cell contains a RH probe (a capacitive sensor with an accuracy of ±1% RH) previously calibrated with saturated salt solutions over the whole RH range. Some values of internal RH, measured continuously by RH probes at T = 21 ± 0.5°C with the mixes CO, CH, BO, and BH, are reported in Table 3 as a function of the age of the materials.

The results reported here, for cement pastes as well as for concretes, are in very good agreement with the RH values given in the literature. For example, RH = 75% was found by Buil for a 50-day concrete containing silica fume and W/C = 0.26 [4]. For a concrete with W/C = 0.44, the value given by the author was RH = 97%. These values are to be compared with RH = 76% obtained at the same age with the concrete BH, and RH = 96.5% found for the concrete BO. Persson [2] found RH ≈ 80% at the age of 28 days and RH ≈ 76% at the age of 3 months (values read on the published figures), for a concrete similar to BH. He found RH ≈ 97% at the age of 28 days and RH ≈ 95% at the age of 3 months for a concrete not very different from BO. For a cement paste with W/C = 0.2 and SF/(C + SF) = 0.08, Sellevold and Justnes found RH = 77% within 1 year [5]. The value exhibited here for CH at the same age is RH = 80%. The results from Wittmann reported by Buil [6] are RH ≈ 99% and RH ≈ 94% for 28-day cement pastes with W/C of 0.4 and 0.3, respectively. The value of RH = 97% obtained here for the cement paste CO (W/C = 0.34) within 28 days seems therefore correct, given the differences in the cement used.

The self-desiccation process depends on mix parameters. For example, it depends on the cement (main influence of the fineness, C_3A content and alkali content [7,8]). Furthermore, it increases with the decrease of the efficient initial water content (role of parameters like W/C, or effective water-to-binder ratio W/[C + k · SF], or water-to-solid ratio,

Table 2
Mineral composition of the cement

Compound	Content (%)
C_3S	57.28
C_2S	23.98
C_3A	3.03
C_4AF	7.59
Gypsum	4.39
$CaCO_3$	1.84
Free CaO	0.53
Na_2O eq.	0.48

Table 3
Internal RH values measured continuously by RH probes at T = 21 ± 0.5°C

	Internal RH (%)			
Age	CO	CH	BO	BH
28 days	97	88.5	97	77.5
50 days	96	84.5	96.5	76
2 months	96	83	96	75.5
3 months	95	81.5	95.5	74.5
6 months	93	80	95	72
1 year	90.5	80	94	69
2 years	87	81	93	64

etc.) and other parameters such as the cement being constant.

In the case of classical materials (W/C ≈ 0.5), self-desiccation remains low. Thus, RH = 95% is reached within 6 months and RH = 94% is reached within 1 year with BO.

HP materials mixed with SF exhibit intense self-desiccation, and this self-desiccation process starts very early. The RH decrease measured in CH and BH is particularly high in the first 2 months. For example, the RH values reached in the concrete BH are RH = 75.5% within 2 months, RH = 72% within 6 months, and RH = 69% within 1 year. In HP materials, at a given age self-desiccation is increased both by lowering W/C and by increasing SF/C. The role of each of these parameters has been widely studied by Jensen and Hansen [9,10] and also by other authors [2,8,11]. For all of the mixes tested here and more particularly for the ordinary materials, the experimental results show that self-desiccation continues for several months.

For durability concerns of reinforced concrete, it is necessary to mention that intense self-desiccation can favour penetration of fluids from the environment through the possible cracks but also through the pore network (capillary suction effect, for example). Areas of low internal RH make water and ion penetration from the environment into the material easier. These agents can be aggressive for concrete or rebars (water containing chloride ions, for example). This point is of importance towards the behaviour of concrete structures exposed to marine environment or to deicing salts. Nevertheless, only the surface layer of the structure is concerned if there is no macrocracking and if intrinsic porosity and permeability of the material are low (inducing very slow transport processes), which is the case with most HP concretes.

In addition, as a result of their intense self-desiccation (which drives their internal RH to a value close to the average RH of a lot of common environmental media) and their fine pore structure (inducing low moisture diffusivity) [8,12,13], HP materials are fairly insensitive to environmental hygral variations over a wide RH range, as will be shown later.

4. Equilibrium moisture properties of the hardened materials

The basic tools for a good understanding, quantification, and prediction of the hygral behaviour of hardened cementitious materials are provided through water vapour desorption and adsorption isotherms (meaning “equilibrium mass water content vs. RH” curves). These curves quantify the water-solid interactions at the origin of mechanical and durability properties and in particular of delayed strains (shrinkage, creep) of the material. There is not a lot of applicable data on cement-based materials, in particular on HP concretes, reported in the literature. Some of the first results on hardened cement pastes (hcp) were published by Feldman in 1968 [14].

In order to obtain such curves, water vapour sorption experiments were carried out at the constant temperature T = 23 ± 0.1°C on thin specimens of the hardened materials studied here.

4.1. Water vapour sorption experiments

Water vapour sorption experiments consist in putting specimens of materials into sealed cells in which the RH is controlled by saturated salt solutions, and in submitting the specimens to step-by-step desorption and adsorption processes. Each step lasts until moisture equilibrium is reached inside the specimen. The specimens are here discs about 3 mm thick, to obtain moisture equilibrium reasonably quickly, with a diameter of about 90 mm for the concretes, and crushed ones ($0.8 < d \leqslant 1$ mm) for the hcp. The slices were wet-sawed from cylinders after curing without water exchange. Given the long duration of both cement hydration (and pozzolanic reaction) and water sorption processes, the specimens were chosen to be 1 year old at the beginning of the test. At this time, very slow kinetics, due to lack of water, space, or unhydrated cement, induce very limited evolution of the degree of hydration. The hydration (and pozzolanic) processes can therefore be assumed to be negligible during the test. This is in agreement with the internal RH values given in Table 3, showing small evolution of RH after 1 year. The mass water content (ratio of the mass of water contained in a specimen to the mass of the dry specimen) is determined by weighing.

The lowest RH tested here is RH = 3% (obtained by virgin silica gel). The dry reference state used to calculate the mass water contents is hence defined by the equilibrium state obtained at RH = 3% and at T = 23 ± 0.1°C. This avoids submitting the specimens to any more or less well-controlled drying process in different conditions from the isothermal desorption process (as oven drying at high temperature and in noncontrolled RH conditions, for example) to reach a dry state. The test starts with a desorption process, as in field conditions where structures undergo drying from their virgin state.

4.2. Experimental water vapour desorption and adsorption isotherms

Water vapour desorption and adsorption isotherms obtained from the experiments previously described at T = 23 ± 0.1°C and for different desorption-adsorption paths are given in Fig. 1 for the hcp CO and CH and in Fig. 2 for the concretes BO and BH. Each plot of the curves is the average of experimental values obtained from at least three specimens.

The results show a considerable hysteresis, extending over the whole RH range. More particularly, desorption-adsorption cycles performed in different hygral ranges scan the hysteretical behaviour of the materials. Inside the area bounded by the complete desorption (from RH = 100%) and adsorption (from RH = 3%) curves, the cycles per-

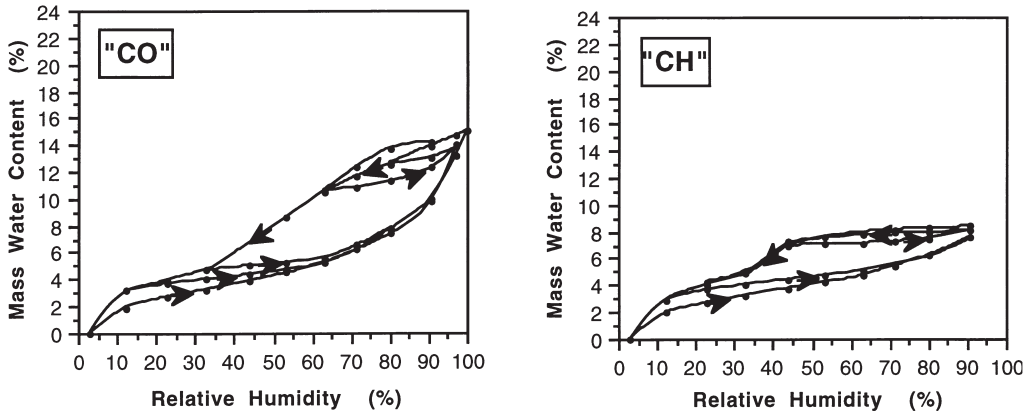

Fig. 1. Water vapour desorption and adsorption isotherms of the hcp CO and CH.

formed illustrate the influence of the hygral path (history) on the measured water content. In particular, the curves obtained in the high RH range are useful for explaining the behaviour of concrete structures in a lot of common environments. For example, in France and neighbouring countries, structures are submitted to daily and season variations where the average conditions are usually RH ≈ 70%.

The influence of mix parameters on the equilibrium moisture properties quantified by the isotherms can also be analysed. For example, the peculiarities of the hygral behaviour of HP materials in the range 50 ⩽ RH ⩽ 90% are pointed out. It can be seen that a low W/C and the use of SF, inducing a very narrow pore network [12,13], modifies the moisture properties of the hardened material. In the high RH range, much lower water contents are measured than for ordinary materials. For cycles running between RH = 50% and RH = 90%, the curves of HP materials show very small water content variations. Such materials are fairly insensitive to environmental moisture variations in this wide RH range. These results are of interest to people concerned with the mechanical behaviour and the durability of HP materials.

Another important point is that with a given cement, below a given RH, the isotherms are identical whatever the mix, when the water contents are calculated by mass of dry hcp contained in the mix, as shown in Fig. 3. It can be seen that in the range where RH ⩾ 44%, the water content measured (and consequently the pore volume and its distribution) is greatly influenced by the mix parameters. On the other hand, for RH ⩽ 44%, the isotherms obtained for the different mixes remain very close, illustrating that in this range (r_p ⩽ 20 Å), moisture equilibrium takes place in a pore structure (internal to C-S-H gel) that is not influenced by the mix parameters [12,13]. This allows identification of the range where calcium silicate hydrates C-S-H, the microcrystallized and microporous gel constituting the bulk solid matrix of cement-based systems, are identical no matter what the mix is.

The analysis of water vapour desorption and adsorption isotherms allows characterization of the nanostructure of hardened materials and therefore of the C-S-H hydrates not accessible by some other technique such as mercury intrusion [8,12,13]. Therefore, these curves constitute essential parameters of developing a model of this nanostructure.

Moreover, water vapour desorption isotherms are a key parameter in the modelling of drying process or drying shrinkage [15,16]. This will be shown in the following parts of this paper through thermodynamics-based macroscopic

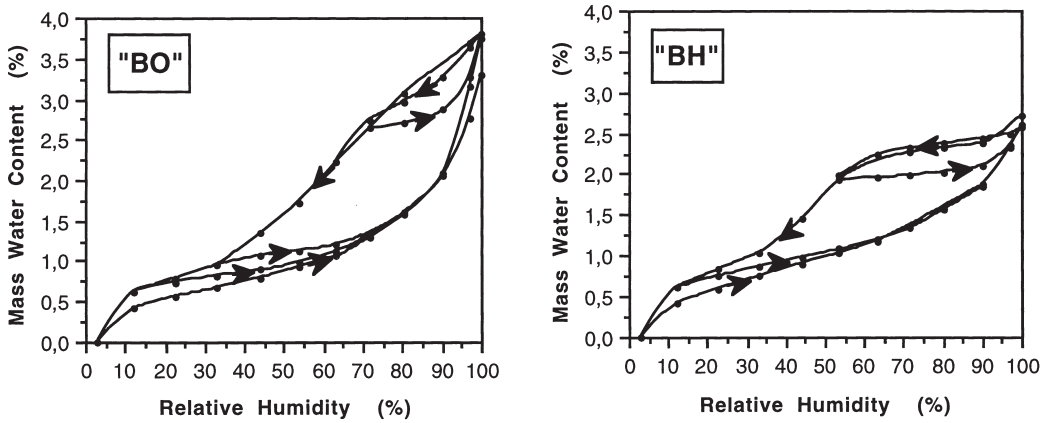

Fig. 2. Water vapour desorption and adsorption isotherms of the concretes BO and BH.

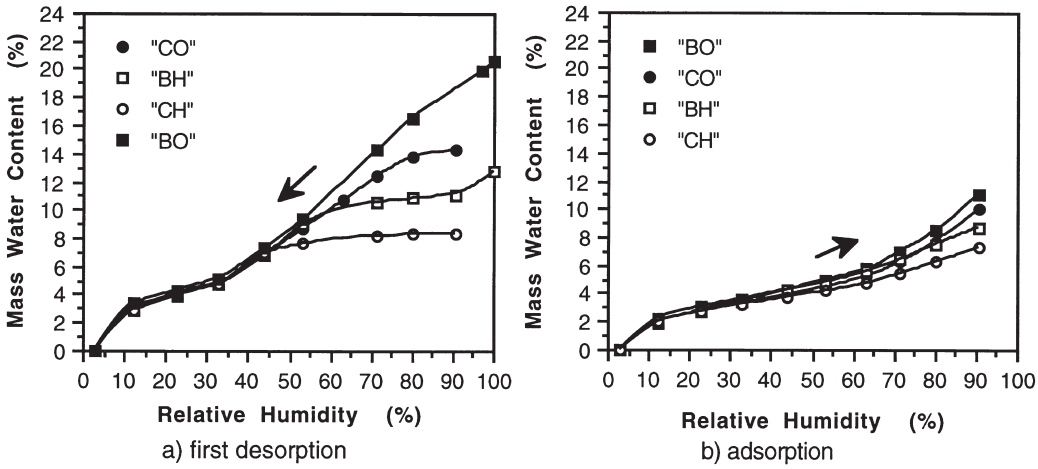

Fig. 3. Water vapour desorption and adsorption isotherms of the hardened materials (water contents are calculated by mass of "dry" hcp contained in the mix).

modelling, where these data, once translated into capillary curve, stand as state equation.

5. Drying shrinkage of the hardened materials

Water removal from the pore structure of hardened materials induces deformations (drying shrinkage). The relationship between RH and this volume change has been well established for a long time. It was first formulated mathematically by Powers [17,18]. However, although drying shrinkage of hcp has been extensively studied for several years and although a lot of models have been proposed in the last ten years [16,19–25], this property does not yet seem to be well understood and remains difficult to predict.

Since Powers, three major mechanisms have been proposed to explain the experimental behaviour of hcp: capillary stress (in pores where menisci are formed due to loss of water), surface free energy (which depends on the amount of adsorbed water [26]), and disjoining pressure (developed in a narrow place where adsorption is hindered [26–28]). In addition, Feldman and Sereda have shown the importance of the movement of interlayer water in C-S-H on drying-wetting deformations [29]. However, how each of these basic mechanisms is involved in the global process and what are the combined effects of the different mechanisms over the entire RH range are not well known at the present time.

5.1. Experimental study

In order to experimentally assess one-dimensional drying shrinkage of the hardened materials studied here, diameter-length change is measured as a function of RH during the water vapour desorption experiments described earlier. The specimens are similar 1-year-old slices as previously described in this section. The diameter-length of the discs is measured by means of dial gauges that have an accuracy of 1 μm. A gauge is put on each disc at the beginning of the test and is not displaced for the duration of the experiment. Equilibrium values of the deformations are calculated by taking as reference the diameter-length measured at RH = 90.4% for each RH step along the desorption process until RH = 12% or RH = 3%, depending on the progress of the experiment. RH = 90.4% appears to be a more relevant reference than RH = 100%, particularly because it is very difficulty to obtain accurate experimental values at RH = 100% given the great influence of temperature and the possible occurrence of sudden and massive water condensation.

The values of one-dimensional drying shrinkage (mean values of experimental data measured on the same set of three specimens) vs. RH, obtained by desorption at T = 23 ± 0.1°C on the hardened materials and calculated by taking the diameter-length at RH = 90.4% as reference, are reported in Fig. 4 for the four mixes CO, CH, BO, and BH. It has to be noted that due to the small deformations of the concretes and the capability of the gauges, it was difficult to obtain a good accuracy in the measures for the concretes, especially below RH = 53.5%.

Shrinkage strains measurements on thin specimens for

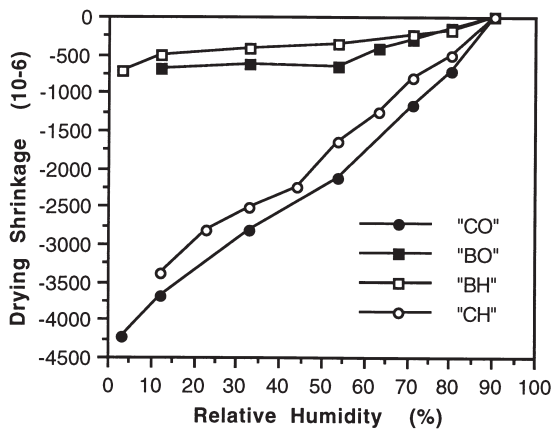

Fig. 4. One-dimensional drying shrinkage of the hardened materials (calculated by taking the diameter-length at RH = 90.4% as reference).

small RH steps has several advantages. First, it is possible to obtain equilibrium values at a given RH within a reasonable time. Second, the conditions of this test are very close to stress-free shrinkage and therefore to the real free deformation of the material at a given RH. This real free deformation is greater than the deformation measured on samples exhibiting surface cracking (as a result of high moisture gradients due to the large dimensions of the samples or to the width of the imposed RH steps) and which depends on the structure geometry.

Fig. 4 shows that drying shrinkage of HP materials is slightly lower than drying shrinkage of ordinary materials at the same RH. The former is about 70% of the latter, when the reference is taken at RH = 90.4%. However, this result is due to a different behaviour restricted to the high RH range. Thus, if deformations are calculated by taking the diameter-length at RH = 12% as reference, it can be seen, for example for the hcp CO and CH, that drying shrinkage vs. RH is roughly identical for the two hcp, at least for RH $\leqslant$ 80.1% (see Fig. 5). This is consistent with the fact that CO and CH contain similar C-S-H hydrate amounts [8,12,13]. In effect, when RH decreases below RH = 76%, pores with $r_p \geqslant 50$ Å are empty. This means that from this stage, C-S-H pores, either internal or external, will be involved in moisture equilibrium and therefore in deformations.

Figs. 4 and 5 indicate that there is a range where a linear relation exists between RH and drying shrinkage. More precisely, it can be seen in Fig. 5 that for the two hcp the relation is linear from RH = 100% up to at least RH = 53.5%. Such a linear relation between RH and shrinkage strains has also been pointed out in the case of autogenous (self-desiccation) shrinkage with the same four mixes [30].

5.2. Theoretical study

In this section, the theoretical modelling of drying shrinkage in nonsaturated porous medium is described. This macro-level modelling is based on the theory of nonlinear poroelasticity proposed by Coussy [31,32]. The aim is to understand and predict the hygromechanical couplings and their effects with a minimum of material parameters that have a clear physical significance and that are accessible by well-defined experiments.

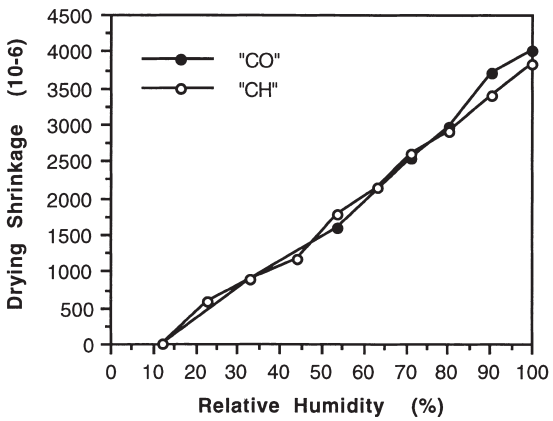

Fig. 5. One-dimensional drying shrinkage vs. RH, obtained by desorption at T = 23 ± 0.1°C on the hcp CO and CH, and calculated by taking the diameter-length at RH = 12% as reference.

5.2.1. Description of the thermomechanical approach: macroscopic state equations

A thermomechanical description of porous media is used, which considers the material as a polyphasic continuum composed of an incompressible solid skeleton and a connected porous space partially saturated by incompressible liquid water (l) and an ideal mixture of water vapour (v) and dry air (a), and where liquid-gas phase changes occur. The processes are assumed to be isothermal here. The two principles of thermodynamics are applied to the elementary volume described, which is an open system because it exchanges fluid matter with the outside.

When assuming both isothermal and poroelastic evolutions, and according to the porous version of the traditional Clausius-Duhem inequality [31,32], the macroscopic state equations of the porous medium are defined from the strain tensor (ε) of the skeleton and the total mass variation (m_i) of fluid (i) due to transport and phase change, which are considered as the state variables of the medium [see Eq. (1)]:

$$\sigma = \frac{\partial \Psi}{\partial \varepsilon} \qquad g_i = \frac{\partial \Psi}{\partial m_i} \tag{1}$$

where $\boldsymbol{\Psi}$ is the global free energy of a unit volume of the porous medium and is assumed to be a thermodynamic potential, depending on the strain tensor ε and on the mass variation m_i. The state equations relate the state variables previously defined to their associated state variables. Hence, as in traditional thermomechanics, the total stress tensor $\boldsymbol{\sigma}$ is the state variable associated with the strain tensor ε. Representative of porous media, the other equation shows that the macroscopic free enthalpy g_i per unit of mass of fluid i is the state variable associated with the corresponding mass variation m_i.

Thanks to the identification with its microscopic traditional definition, g_i can be replaced by the partial pressure p_i of fluid i, experimentally and physically more convenient ($dg_i = dp_i/\rho_i$, where ρ_i is the density of fluid i).

5.2.2. Nonlinear elastic constitutive law

To account for significant variations of interstitial pressures occurring in nonsaturated porous media, a nonlinear elastic constitutive law is derived from Eq. (1). This constitutive law is written as a matricial relation between increments of stresses and pressures on the one hand, and increments of strains and mass variations on the other hand, as in Eq. (2):

$$\begin{bmatrix} d\sigma \\ dp_i \end{bmatrix} = \begin{bmatrix} \boldsymbol{C} & (-\boldsymbol{bM})^t \\ -\boldsymbol{bM} & \boldsymbol{M} \end{bmatrix} \begin{bmatrix} d\varepsilon \\ dm_j/(\rho_j) \end{bmatrix} \tag{2}$$

In this relation stands a symmetric matrix $\boldsymbol{C}$, corresponding to the undrained ($dm_j = 0$) elastic relation between mechanical stress and strain. Another symmetric matrix $\boldsymbol{M} = (M_{ij})$, called matrix of Biot's moduli, quantifies the mutual

influence between mass variations m_j divided by the respective density ρ_j and partial pressures p_i. The hygromechanical coupling, between mechanical state variables and state variables of interstitial fluids, is taken into account through the vector of Biot's coefficients $\boldsymbol{b} = (b_i)$.

All of the tangent moduli appearing in Eq. (2) are considered and must be identified as functions of the state variables $\boldsymbol{\varepsilon}$, m_l, m_v, and m_a. However, thanks to the postulated existence of a unique potential $\boldsymbol{\Psi}$, they are linked by the Maxwell's symmetric relations on partial derivatives [33]. In addition to the Maxwell's relations, some microscopic assumptions are made (solid and liquid incompressibility, dry air and water vapour considered as ideal gases) in order to simplify the dependence of the moduli on the state variables.

Finally, the isotropic macroscopic constitutive law can be written in the simplified form shown in Eq. (3) and Eq. (4):

$$d\sigma = K_0 d\varepsilon + b_l(p_c)dp_c - dp_g \tag{3}$$

$$dp_c = -M\left[-b_l(p_c)d\varepsilon + \frac{dm_l}{\rho_l}\right] \tag{4}$$

where $\sigma = tr\boldsymbol{\sigma}/3$ is the average stress, ε is the volumetric strain, M is the capillary modulus, p_g is the total pressure of the gas mixture, $p_c = p_g - p_l$ is the capillary pressure, and ρ_l is the (constant) liquid water density. K_0 is the drained ($dp_c = dp_g = 0$) bulk modulus, defined as shown in Eq. (5):

$$K_0 = \frac{E}{3(1-2\nu)} \tag{5}$$

where E is the Young's modulus and ν is the Poisson's ratio (in drained conditions).

As shown by Eq. (3), the whole model is entirely determined as soon as the relation between b_l and p_c is known. According to Eq. (4), the knowledge of such a relation can be obtained via the experimental measurement of the capillary pressure (p_c) as a function of ε and the liquid mass variation (m_l). It is also important to stress that, due to the existence of a unique potential ($\boldsymbol{\Psi}$), the same coupling function $b_l = b_l(p_c)$ appears both in the mechanical equation [Eq. (3)] and in the hygral relation [Eq. (4)].

5.3. Simplifying assumptions and final determination of the model

5.3.1. The capillary curve as state equation

After all of these previous theoretical considerations, and thanks to the assumptions made (particularly the assumption of liquid and solid incompressibility), the only missing information is the determination of the capillary pressure (p_c) as a function of the state variables ε and m_l. This state equation, which is a constitutive law replacing in the macroscopic formulation the microscopic equilibrium of the capillary menisci, is introduced into the modelling as experimental data. In order to fit more easily the experimental data, it is convenient to use the liquid water saturation S_l instead of m_l in the expression of the capillary pressure. The liquid water saturation (S_l) is defined by Eq. (6):

$$S_l = \frac{\phi_l}{\phi} \tag{6}$$

where ϕ is the total porosity and ϕ_l is the volumetric content of liquid water. So that p_c can finally be considered as a function of the volumetric strain ε and the liquid water saturation S_l [see Eq. (7)]:

$$p_c = p_c(\varepsilon, S_l) \tag{7}$$

With the additional hypothesis [30] of Eq. (8):

$$b_l = S_l \tag{8}$$

and thanks to Eq. (4) expressed with S_l instead of m_l, it can be shown that p_c becomes independent of the volumetric strain ε and is only determined by the liquid saturation S_l, as seen in Eq. (9):

$$p_c = p_c(S_l) \tag{9}$$

The state equation [Eq. (9)] also called capillary curve, which is a more restrictive version of the previous state equation [Eq. (7)], is in good agreement with the experimental measurements, giving the evolution of the capillary pressure with the liquid saturation as an exhaustive information (on a monotone drying path).

5.3.2. Determination of the model through water vapour desorption isotherms

The liquid saturation S_l can be calculated from the mass water content w of the material, by using the relation shown in Eq. (10):

$$S_l = \frac{w\rho_s}{\phi\rho_l} \tag{10}$$

where ρ_s is the apparent density of the material. Moreover, the Kelvin's equation expressing the liquid-vapour equilibrium in atmospheric conditions $p_g = p_{atm}$ gives the relation between p_c and the relative humidity (h) [see Eq. (11)]:

$$p_c = -\frac{\rho_l RT}{M_v}\ln h \tag{11}$$

where R is the gas constant and M_v is the molar mass of water. Therefore, the capillary curve [Eq. (9)] can be deduced from experimental water vapour desorption isotherm. And, as it is shown in Fig. 6 it is possible to deduce a general determination of the whole model from a single specific experiment. Any relation between state variables obtained from water vapour desorption experiments is in fact linked to the particular conditions of the experiments (constant total gas pressure, no stress). However, due to Eq. (9), the experimental data can be considered as general constitutive law, valid every time and in every case, when expressed in terms of a relation between p_c and S_l.

When introducing in Eq. (3) the boundary conditions of the experiment ($p_g = p_{atm}$ no stress) and when combining this equation with the identification equation [Eq. (8)], Eq. (12) is obtained:

$$K_0 d\varepsilon = -S_l dp_c \tag{12}$$

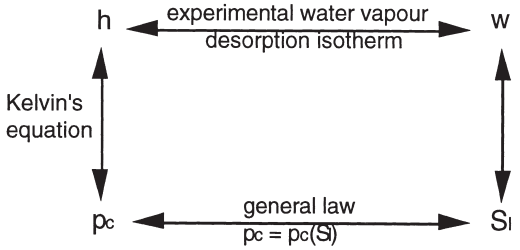

Fig. 6. General determination of the whole model from a single specific experience.

which expresses that capillary tension induces compressive stress of the solid skeleton. When combining Eq. (12) with Kelvin's equation [Eq. (11)], the constitutive law reads as Eq. (13):

$$d\varepsilon = \frac{\rho_l RT}{K_0 M_V} \frac{S_l}{h} dh \tag{13}$$

Therefore drying shrinkage strains can be calculated from the measure of the water vapour desorption isotherm and of the bulk modulus of the material. Since the deformations are isotropic, the one-dimensional drying shrinkage can be deduced from Eq. (13) as $d\varepsilon_d = d\varepsilon/3$.

5.4. Prediction of one-dimensional drying shrinkage of hcp: Comparison with experiments

In Fig. 7, the predicted drying shrinkage given by the modelling previously described is plotted vs. RH and is compared with the experimental equilibrium values of drying shrinkage observed for the hcp CO and CH (as explained earlier). The Young's modulus was 17 GPa for CO and 21 GPa for CH. The Poisson's ratio was assumed to be $\nu = 0.25$. Such comparison has already been performed by Carmeliet on cellulose cement composite [34].

A very close agreement is obtained, in particular for CH, between calculated and experimental data in the range where RH $\geqslant$ 44%, and both curves are linear in this range. In the range where RH $\leqslant$ 44%, the calculated values diverge from the experimental ones. Mechanisms other than capillary stresses become probably prominent in this range, like surface free energy [26]. When RH $\leqslant$ 44%, pores with $r_p \geqslant 20$ Å are emptied (see earlier explanation). The water liquid phase is disconnected and an important part of the specific surface area is indeed covered with an adsorbed water layer. Therefore, a model based on capillary effects is probably not the most suitable in the low RH range. The drying shrinkage results therefore point out again the two ranges, above and below RH = 44%, previously found through the sorption isotherms. Moreover, the calculated values confirm also the similar values experimentally obtained on the hcp CO and CH.

6. Drying process in the hardened materials

Isothermal drying occurs in concrete when the material is submitted to a lower environmental RH than its internal RH.

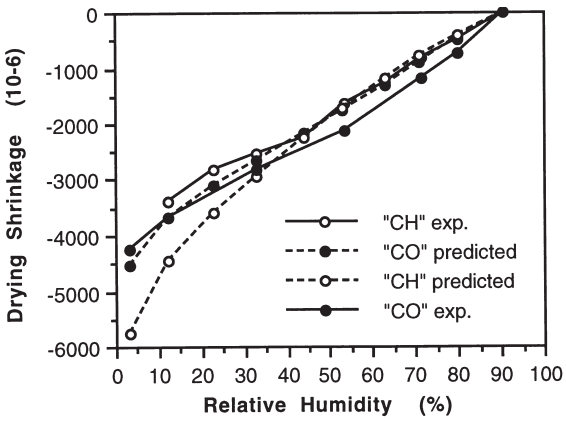

Fig. 7. Comparison between observed and predicted one-dimensional drying shrinkage of the hcp.

This thermodynamic imbalance entails a diffusion of the water vapour through the air contained in the sample. An evaporation of the liquid water occurs simultaneously within the sample in order to maintain the liquid-vapour (isothermal) equilibrium. Consequently, the liquid water pressure does not remain constant and a liquid water movement also occurs within the sample. Furthermore, the total pressure of the gas phase (water vapour + dry air) does not remain constant due to the combination of the diffusion process and the evaporation. The process ends when the balance between external and internal RH and gas pressure is restored.

Moisture transport is a very slow process in the very fine pore network of cementitious materials. The time required to reach moisture equilibrium in a sample depends on the thickness of the sample and on the RH step. Moisture equilibrium state can be reached after a few months and up to more than 1 year for the few mm thick specimens described earlier, depending on the RH range. It is generally accepted that the macroscopic moisture transport in isothermal conditions can be described in cement-based materials using a nonlinear diffusion-type equation, where the coefficient, called moisture diffusivity, includes all of the mechanisms related to liquid or gas flow. Nevertheless, it is difficult on the basis of such a global coefficient only to clear what are the different processes involved, given the complex interaction of liquid and vapour phases in the pore system, and to determine what are the key parameters in these processes. Furthermore, the measured moisture diffusivity depends greatly on the method used [35]. It is therefore still necessary to come back to the basic laws in order to better understand the drying process and to point out the key parameters that one must experimentally assess.

6.1. Experimental moisture content distribution in drying samples

Samples (Ø16 × 10 cm) of the four mixes were submitted to drying at RH = 50 ± 5% and T = 20 ± 1°C. The materials were 2 years old at the beginning of the test to avoid self-desiccation influence on the drying process. The samples were sawed from cylinders (previously protected

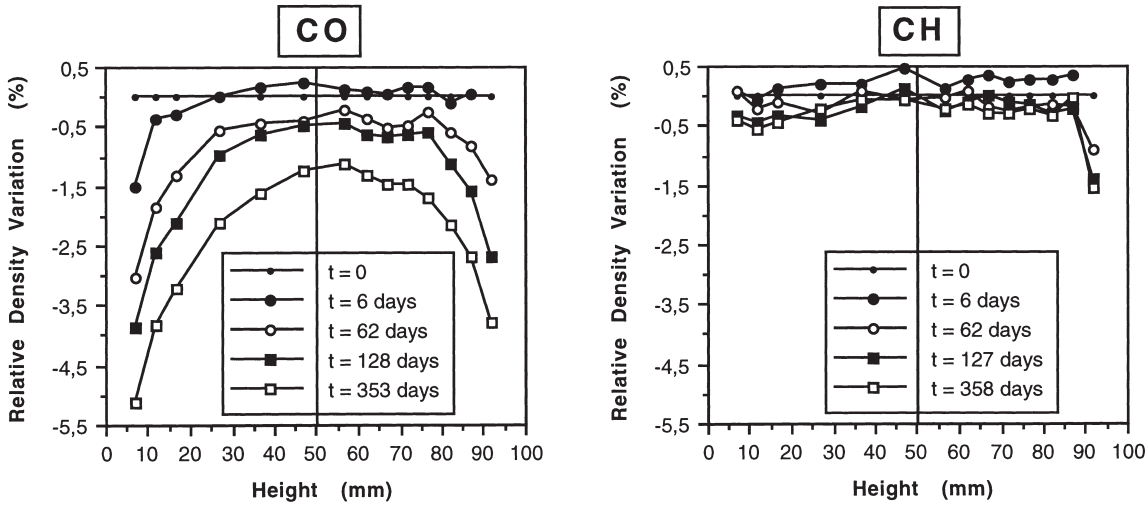

Fig. 8. Moisture content distribution in drying samples of the hcp, determined by gamma-ray measurements.

from moisture exchange) and wrapped in two superposed aluminium foil sheets prior to the drying process (except the two symmetrical plane surfaces) to perform one-dimensional drying test. Gamma-ray attenuation measurements were performed on the drying samples to determine their moisture content distribution (profile).

The moisture content distribution in the samples and its evolution as a function of drying time is given vs. the height of the samples in Fig. 8 for the hcp and in Fig. 9 for the concretes. The results highlight a very different behaviour in these drying conditions (RH = 50 ± 5% and T = 20 ± 1°C) for ordinary and HP materials. The moisture content distributions obtained for CO and BO show gradients shifting as a function of drying time. The moisture content distributions obtained for CH and BH show practically no evolution, even after 1 year of drying.

This difference is due first to the fact that ordinary and HP materials are in a very different moisture state at the initial time of this drying experiment. The test begins after 2 years of storage without moisture exchange with the environment. Therefore, at the initial time of the test, the self-desiccation process has induced an internal RH value of 93% for BO, 87% for CO, 81% for CH, and 64% for BH (Table 3). When the materials are submitted to RH = 50 ± 5%, the prevailing moisture gradient between core and cover of the sample is very small in HP materials compared to ordinary samples. The moisture flow is hence respectively reduced.

Moreover, the moisture diffusivity of the materials decreases with RH in the range involved in this test [8,13,35]. The RH range involved, for example, for BO is 93–50% and for BH is 64–50%. Hence, there is a zone (corresponding to RH > 64%) along the drying process where the moisture diffusivity will be higher for BO than for BH and where the drying kinetics will consequently be faster.

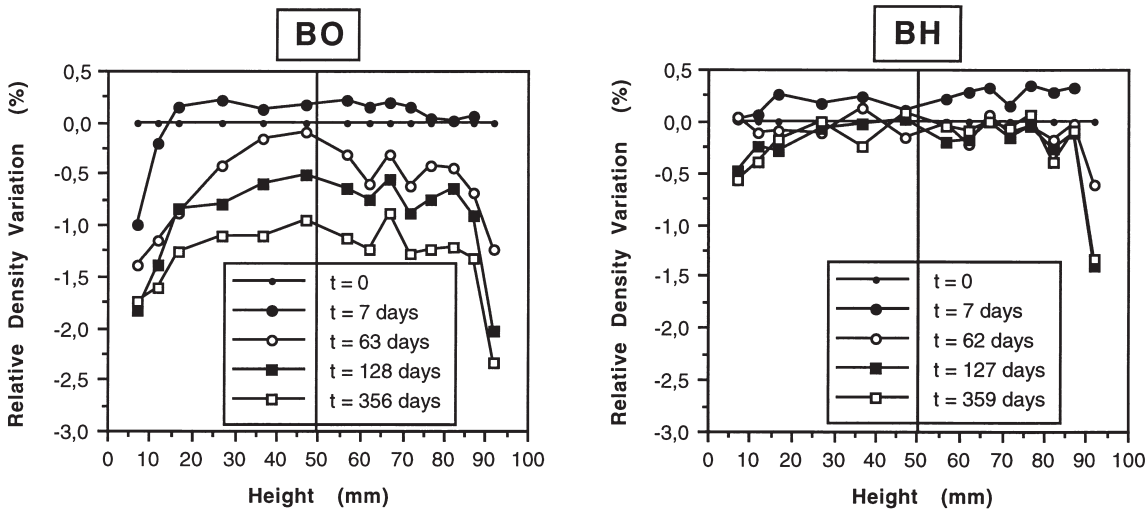

Fig. 9. Moisture content distribution in drying samples of the hardened concretes, determined by gamma-ray measurements.

Furthermore, the capillary pore structure involved in the drying test described here is finer in the HP mixes [8,12,13]. This is an other cause of slowing the drying kinetics.

6.2. Modelling of isothermal drying process and identification of material properties

In this section a model is proposed that accounts for the isothermal drying process as previously depicted and constitutes a further development of previous work [31,32,36]. The deformation of the solid skeleton does not influence significantly the drying process and is not considered in what follows.

6.2.1. Governing equations of isothermal drying

The mass balance equations for *l*, *v*, and *a* read, respectively [see Eq. (14)]:

$$\begin{cases} \dfrac{\partial}{\partial t}(\phi \rho_l S_l) = -\mathrm{div}(\phi S_l \rho_l \mathbf{v_l}) - \mu_{l\to v} \\ \dfrac{\partial}{\partial t}(\phi \rho_v (1-S_l)) = -\mathrm{div}(\phi (1-S_l)\rho_v \mathbf{v_v}) + \mu_{l\to v} \\ \dfrac{\partial}{\partial t}(\phi \rho_a (1-S_l)) = -\mathrm{div}(\phi (1-S_l)\rho_a \mathbf{v_a}) \end{cases} \quad (14)$$

In Eq. (14), $\phi_l = \phi S_l$ and $\phi_g = \phi(1 - S_l)$ represent the ratios of the material volume occupied respectively by the liquid *l* and the gas *g*. Furthermore $\mu_{l\to v}$ denotes the rate of mass of liquid water changing into vapour per unit of overall material volume. Finally, $\mathbf{v_i}$ is the velocity of fluid *i*.

The transport of liquid water and that of the gas are assumed to be governed by Darcy's law, which reads (i = l or *g*) for an isotropic porous medium [see Eq. (15)]:

$$\phi_i \mathbf{v_i} = -\frac{K}{\eta_i} k_{ri}(S_l)\,\mathbf{grad}\, p_i \quad (15)$$

In Eq. (15), *K* is the permeability of the porous material, which is an intrinsic property of the material independent of the saturating phases. η_i and $k_{ri}(S_l)$ are, respectively, the dynamic viscosity and the relative permeability associated with fluid *i*. Assuming that the gas is an ideal mixture, its pressure p_g is the sum of the pressures of its constituents $p_g = p_v + p_a$. When Eq. (15) applies to the gas phase, $\mathbf{v_g}$ is the molar averaged velocity of its constituents, reading $\mathbf{v_g} = C_v \mathbf{v_v} + C_a \mathbf{v_a}$, where C_j is the molar ratio of constituent $j = a$ or *v*, and reads $C_j = p_j/p_g$, since the gas phase is assumed to be an ideal mixture. The choice of the averaged molar velocity rather than the massive one relies on thermodynamic considerations [31,37] and has also been adopted elsewhere [38].

Finally the relative diffusion process of water vapour and dry air phases relative to the gaseous mixture are assumed to be governed by Fick's law, which reads ($j = a$ or *v*) as seen in Eq. (16):

$$\phi_g(\mathbf{v_j} - \mathbf{v_g}) = -F(S_l)\frac{D_{va}(T)}{p_g C_j}\,\mathbf{grad}\, C_j \quad (16)$$

with Eq. (17)

$$D_{va}(T) = 0.217\, p_{atm}\left(\frac{T}{T_0}\right)^{1.88} \quad (17)$$

Fick's law as formulated by Eq. (16) agrees with the microscopic expression, which can be directly derived from the kinetic theory of gases [39]. Furthermore Eq. (16) accounts explicitly for the inversely proportional dependence of the relative flow of constituent *j* to the total gas pressure p_g. This dependence comes from the expression adopted for the diffusion coefficient $D_{va}(T)/p_g$ of the water vapour in the air given by de Vries and Kruger [40] (with D_{va}/p_g in $cm^2 \cdot s^{-1}$, T in K, $T_0 = 273$ K, and $p_{atm} = 101325$ Pa). In addition, the factor $F(S_l)$ accounts simultaneously for the tortuosity effects and the reduction of space offered to gas diffusion [41].

Eq. (14) to Eq. (16) have to be completed by the state equations. The water vapour and the dry air are assumed to be ideal gases, while the liquid pressure is governed by the capillary curve already introduced in this paper. Therefore the state equations read as shown in Eq. (18):

$$p_j M_j = RT\rho_j \quad \text{and} \quad p_g - p_l = p_c(S_l) \quad (18)$$

where M_j is the molar mass of constituent *j*. Finally, assuming that the liquid water and its vapour remain permanently in local thermodynamic equilibrium, the rate of evaporation is governed by the equality of their Gibbs potentials at each time. When differentiated, this equality leads to the well known isothermal Clapeyron's law [see Eq. (19)]:

$$\frac{dp_v}{\rho_v} - \frac{dp_l}{\rho_l} = 0 \quad (19)$$

Table 5
Best parameters of Eq. (20) for each mix

	Mix			
	BO	BH	CO	CH
a (MPa)	18.6237	46.9364	37.5479	96.2837
b (−)	2.2748	2.0601	2.1684	1.9540

Table 4
Total porosity and apparent density of the hardened materials

	Mix			
	BO	BH	CO	CH
Total porosity ϕ (%)	12.2	8.2	30.3	20.4
Apparent density ρ_s ($kg \cdot m^{-3}$)	2285	2385	1717	2086

Table 6
Intrinsic permeability obtained by fitting numerical weight loss on experimental results

	Mix			
	BO	BH	CO	CH
Intrinsic permeability *K* (m^2)	$3 \cdot 10^{-21}$	$5 \cdot 10^{-22}$	$1 \cdot 10^{-21}$	$0.3 \cdot 10^{-22}$

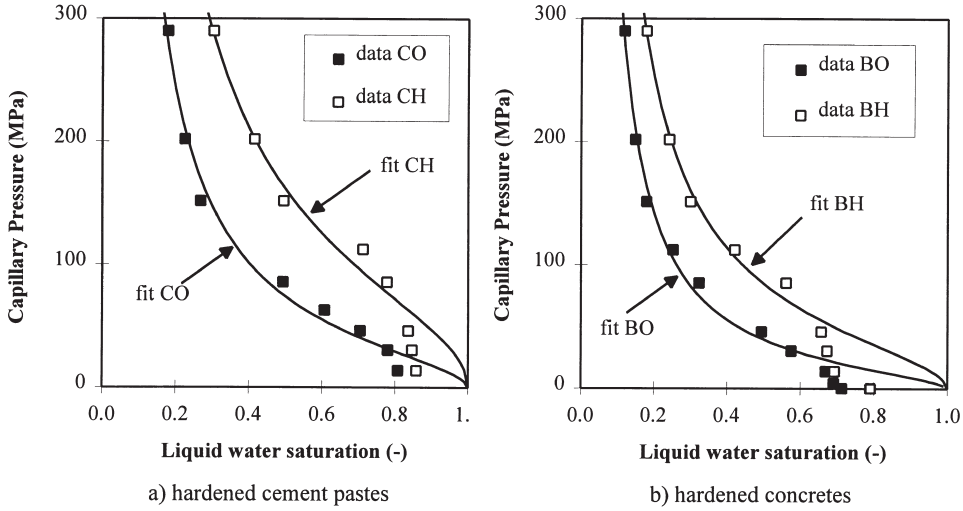

Fig. 10. Capillary pressure vs. liquid water saturation.

6.2.2. Identification of material properties

As indicated previously, the capillary curve can be deduced from the experimental water vapour desorption isotherm by using Eq. (10) and Eq. (11). Using the corresponding data given elsewhere [8,12,13] for the mixes CO, CH, BO, and BH (recalled in Table 4), one obtains some experimental plots of the capillary curves as given in Fig. 10.

A good fit of the capillary curve is obtained through Eq. (20):

$$p_c(S_l) = a(S_l^{-b} - 1)^{1-1/b} \tag{20}$$

The best fits for parameters a and b involved in Eq. (20) are given in Table 5. The corresponding functions are reported in Fig. 10 and can be compared with the experimental data. In looking for the best fit, the experimental data corresponding to the lowest capillary pressures (corresponding to the highest RH) have not been accounted due to their weak reliability.

The relative permeabilities to water [42] and to gas [43] are approached using Mualem's model with $b = 1/m$, which reads as Eq. (21) and Eq. (22):

$$k_{rl}(S_l) = \sqrt{S_l}(1-(1-S_l^{1/m})^m)^2 \tag{21}$$

$$k_{rg}(S_l) = \sqrt{1-S_l}(1-S_l^{1/m})^{2m} \tag{22}$$

Using these expressions and the values given in Table 5 for parameter b, the relative permeabilities to water and gas for the different analysed materials are represented in Fig. 11.

Finally, the expression of the resistance factor $F(S_l)$ involved in Fick's law [Eq. (16)] is the one given by Millington [44, see Eq. (23)]:

$$F(S_l) = \phi_g^{4/3}(1-S_1)^2 = \phi^{4/3}(1-S_l)^{10/3} \tag{23}$$

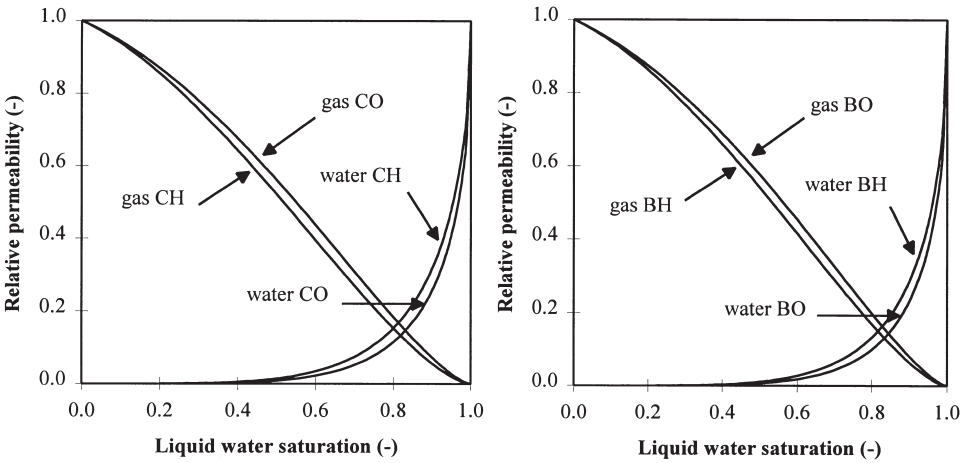

Fig. 11. Relative permeabilities to water and to gas.

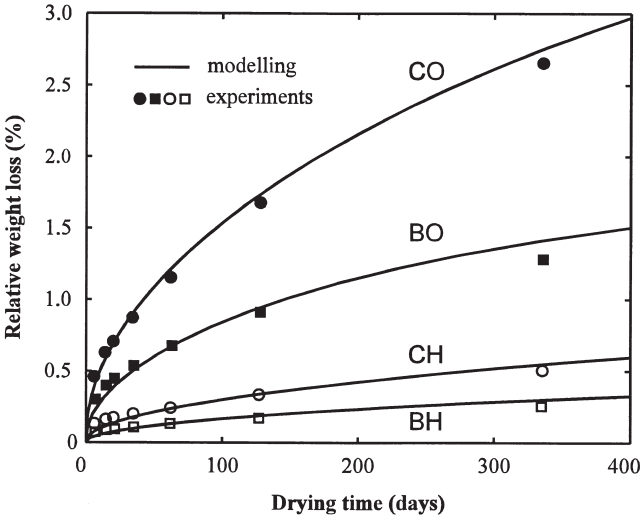

Fig. 12. Fit of numerical relative weight loss on experimental results.

6.3. Isothermal drying process: comparison between modelling and experiments

6.3.1. Numerical resolution

The system of Eq. (14) to Eq. (19) has been numerically solved using the finite volume method [45]. The finite volume method is well suited here since the discrete form of the mass balance laws [Eq. (14)] is strictly satisfied. The four unknown variables in the adopted discretization scheme are the liquid water saturation S_l, the water vapour pressure p_v, the dry air pressure p_a, and the rate of liquid mass evaporation ($\mu_{p\to v}$). An implicit approximation of the normal derivative ensuring the best stability of the scheme is used. The resulting nonlinear system is solved through a standard Newton-Raphson method. See earlier work [37] for further information.

The drying process and the geometry of the samples of CO, CH, BO, and BH simulated here are described previously. The initial state has to be specified through the initial value of the (atmospheric) gas pressure and that of the internal RH of the 2-year-old materials (see Table 3). These two initial conditions allow computation of initial water vapour and dry air pressure. Lastly, the liquid water saturation at the beginning of the drying process can be calculated from the Kelvin's equation at atmospheric pressure [Eq. (11)]. Finally, the boundary conditions consist in imposing RH = 50% and a gas pressure equal to the constant atmospheric pressure at the boundary of the samples.

Table 7
Intrinsic permeability obtained with Katz-Thompson model

	Mix	
	CO	CH
Intrinsic permeability K (m^2)	$3\cdot10^{-21}$	$2\cdot10^{-22}$

6.3.2. Identification of the intrinsic permeability: discussion of the results

The last material property remaining to be specified is the key parameter represented by the intrinsic permeability K. This parameter is identified by comparing the relative weight loss of the sample versus time predicted by the model and the one experimentally recorded. This comparison consists in determining the value of K, which leads to the best account of the observed data. The values obtained for the different hcp and concretes are summarized in Table 6. The experimental and the predicted relative weight losses are presented in Fig. 12. Note that the relevance of the proposed modelling can be appreciated a posteriori through its accuracy to represent a lot of experimental plots, provided the identification of a single material property, the intrinsic permeability K.

Note also the good agreement in order of magnitude of the permeability of the hcp CO and CH predicted by the proposed model (Table 6) and its evaluation by using the Katz-Thompson model [46] as performed previously [8] (Table 7).

The numerical calculations have shown that, contrary to usual assumptions, the gas pressure does not remain con-

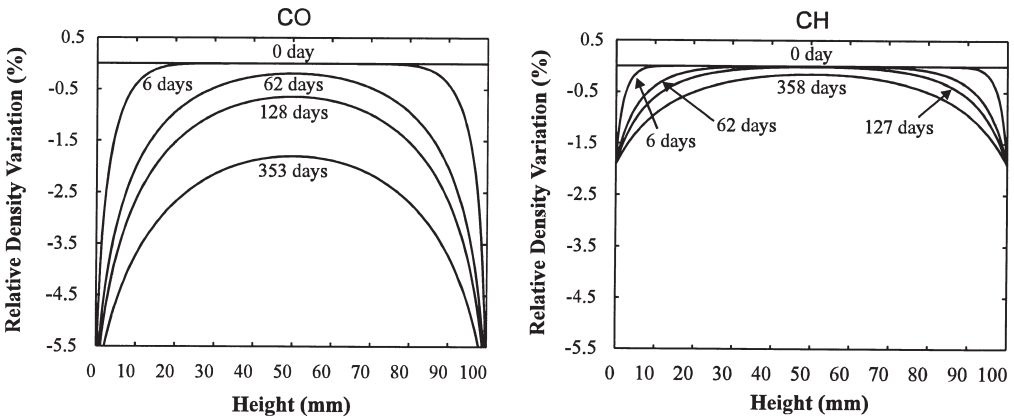

Fig. 13. Liquid water saturation profiles at different times in the hardened concretes.

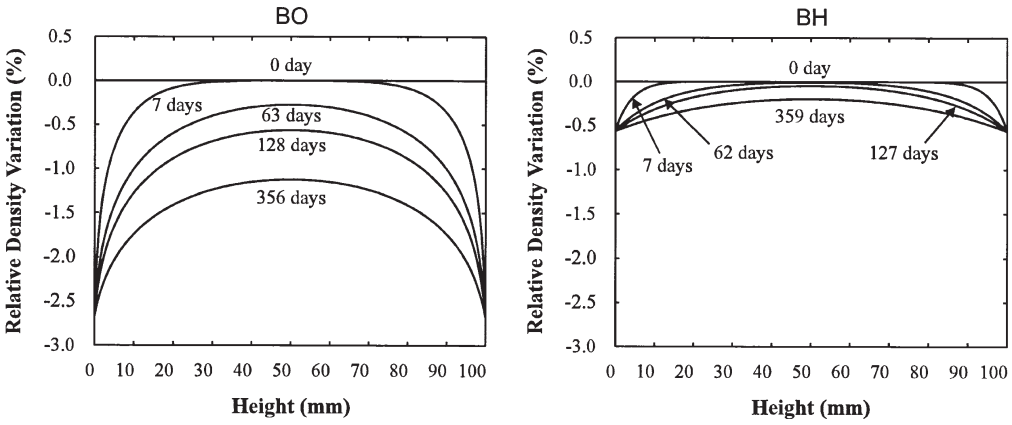

Fig. 14. Liquid water saturation profiles at different times in the hcp.

stant during drying. An overpressure arises on the border layer of the sample and progresses towards its centre as time passes. Due to the low value of the intrinsic permeability, this overpressure takes a very long time to vanish. Finally the profiles presented in Figs. 13 and 14 show the relative density variations predicted by the model for the various tested materials during the drying process at RH = 50%. These are very similar to results obtained experimentally through gamma-ray attenuation measurements (Figs. 8 and 9). These results confirm the determining influence of the initial RH gradient between the boundary and the core of the sample, as suggested by the experimental results. Thus, the small gradients prevailing inside the HP materials induce reduced transfers and flat profiles.

In conclusion, it can be said that once the porosity, capillary curve, and intrinsic permeability (from experiment or, for example, by means of the Katz-Thompson model) are determined, one has a predicting model. This tool can be used to quantify the hygral state of a porous material along its drying process. In particular, this model is able to provide weight loss and moisture content profiles.

7. Conclusions

Water vapour sorption isotherms characterize the equilibrium moisture properties of hardened materials. The experimental curves obtained on ordinary and high-performance hcp and concretes have pointed out the range where the curves are identical whatever the mix (RH $\leqslant$ 44%). In the high RH range, the influence of mix parameters becomes obvious. A different behaviour is observed for HP materials when the RH varies in this range. More exactly, between RH = 50% and RH = 90%, very small evolutions of the mass water content are registered for these materials.

Moreover, the water vapour desorption isotherm, once translated into capillary curve, appears as state equation in the thermodynamics-based modelling of drying process or of its consequences such as drying shrinkage.

As shown in this paper, to predict one-dimensional drying shrinkage of cementitious materials as a function of RH, only their water vapour desorption isotherm and their bulk modulus need to be experimentally determined. The modelling based on capillary stresses, proposed here, seems to be quite suitable at least for engineering purposes, given the close agreement obtained in the range RH $\geqslant$ 44% between predicted and observed values for the two hcp tested.

The other key parameter involved in moisture transfer processes, and more generally in every transport process, is the intrinsic permeability of the material. Once the porosity, capillary curve, and intrinsic permeability of the material are determined, the model presented here is able to predict the hygral state of a porous material along its isothermal drying process. Thus, the moisture profiles calculated for the different hardened materials studied agree very well with the profiles obtained experimentally by gamma-ray attenuation measurements (evolution of the moisture content and its gradient as a function of time). The results show a very different behaviour between ordinary and HP materials. The specific behaviour of HP materials results mainly from their strong self-desiccation that has induced a low internal RH within the samples before the beginning of the drying process at RH = 50%. Thus, the RH difference (gradient) between the core and the surface of the sample, and therefore the hygral potential, is smaller in the HP materials compared to ordinary materials. The moisture transfers are therefore reduced in BH and CH, as indicated by the smaller weight losses and the profiles (little evolution of the water content inside the material).

References

[1] S. Miyazawa, P.J.M. Monteiro, Volume change of high-strength concrete in moist conditions, Cem Concr Res 26 (4) (1996) 567–572.
[2] B. Persson, Hydration and strength of high performance concrete, ACBM 3 (1996) 107–123.
[3] L.E. Copeland, G.H. Bragg, Self-desiccation in Portland cement paste, Bull Portland Cem Association 52 (1955) 1–11.
[4] M. Buil, Comportement physico-chimique du système ciment-fs, Annales de l'ITBTP 483 (271) (1990) 19–29.

[5] E.J. Sellevold, H. Justnes, High strength concrete binders. Part B: Non evaporable water, self-desiccation and porosity of cement pastes with and without condensed silica fume, in: Proceedings of the 4th ACI/CANMET Int. Conf. on fly ash, silica fume, slag and natural pozzolans in concrete, Vol. 2, Istanbul, Turkey, 1992, ACI SP 132-52, pp. 887–902.
[6] M. Buil, Contribution à l'étude du retrait de la pâte de ciment durcissante, LCPC Report 92, 1979.
[7] E. Atlassi, Influence of cement type on the desorption isotherm of mortar, Nordic Concrete Research 10 (1991) 25–36.
[8] V. Baroghel-Bouny, Characterization of Cement Pastes and Concretes—Methods, Analysis, Interpretations, Laboratoire Central des Ponts et Chaussées, Paris, 1994 (in French).
[9] O.M. Jensen, P.F. Hansen, Autogenous relative humidity change in silica fume-modified cement paste, Advances in Cement Research 7 (25) (1995) 33–38.
[10] O.M. Jensen, P.F. Hansen, Autogenous deformation and change of the relative humidity in silica fume-modified cement paste, ACI Materials Journal 95 (6) (1996) 539–543.
[11] P. MacGrath, R.D. Hooton, Self-desiccation of Portland cement and silica fume modified mortars, in: S. Mindess (Ed.), Ceramic Transactions, Advances in Cementitious Materials, Vol. 16, Am. Ceram. Soc., 1990, pp. 489–500.
[12] V. Baroghel-Bouny, T. Chaussadent, Pore structure and moisture properties of cement-based systems from water vapour sorption isotherms, in: Proceedings of MRS 1994 Fall Meeting, Vol. 370, Boston, Materials Research Society, 1995, pp. 245–254.
[13] V. Baroghel-Bouny, Texture and moisture properties of ordinary and high-performance cementitious materials, in: J.P. Bournazel, Y. Malier (Eds.), Proceedings of the International RILEM Conference Concrete: From Material to Structure, September 11–12, 1996, Arles, France, RILEM, 1998, pp. 144–165.
[14] R.F. Feldman, Sorption and length-change scanning isotherms of methanol and water on hydrated Portland cement, in: Proceedings of the 5th International Congress on the Chemistry of Cement, Vol. 3, Cement Association of Japan, Tokyo, 1968, pp. 53–66.
[15] D.P. Bentz, D. Quenard, V. Baroghel-Bouny, E.J. Garboczi, H.M. Jennings, Modelling drying shrinkage of cement paste and mortar. Part 1: Structural models from nanometers to millimeters, Materials and Structures 28 (1995) 450–458.
[16] T. Shimomura, K. Maekawa, Analysis of the drying shrinkage behaviour of concrete using a micromechanical model based on the micropore structure of concrete, Magazine of Concrete Research 49 (181) (1997) 303–322.
[17] T.C. Powers, Mechanisms of shrinkage and reversible creep of hardened cement paste, in: Proceedings of the International Symposium of the Structure of Concrete and Its Behaviour under Load, Cement and Concrete Association, London, 1965, pp. 319–344.
[18] T.C Powers, The thermodynamics of volume change and creep, Materials and Structures 1 (6) (1968) 487–507.
[19] P. Acker, Retraits et Fissurations du Béton: Causes, Mécanismes, Modèles, AFPC, Paris, 1991.
[20] W. Hansen, Drying shrinkage mechanisms in Portland cement paste, J Am Ceram Soc 70 (5) (1987) 323–328.
[21] J.A. Almudaiheem, An improved model to predict the ultimate drying shrinkage of concrete, Magazine of Concrete Research 44 (159) (1992) 81–85.
[22] M.Y. Han, R.L. Lytton, Theoretical prediction of drying shrinkage of concrete, J Materials Civil Engineering 7 (4) (1995) 204–207.
[23] L. Granger, J.M. Torrenti, P. Acker, Thoughts about drying shrinkage: Scale effects and modelling, Materials and Structures 30 (1997) 96–105.
[24] Z.P. Bazant, J.K. Kim, Consequences of diffusion theory for shrinkage of concrete, Materials and Structures 24 (1991) 323–326.
[25] Y. Xi, H.M. Jennings, Shrinkage of cement paste and concrete modelled by a multiscale effective homogeneous theory, Materials and Structures (30) (1997) 329–339.
[26] F.H. Wittmann, Interaction of hardened cement paste and water, J Am Ceram Soc 56 (8) (1973) 409–415.
[27] Z.P. Bazant, Thermodynamics of hindered adsorption and its implications for hardened cement paste and concrete, Cem Concr Res 2 (1) (1972) 1–16.
[28] C.F. Ferraris, F.H. Wittmann, Retrait de la pâte de ciment durcie, Chantiers 4 (1987) 289–292.
[29] R.F. Feldman, P.J. Sereda, A model for hydrated Portland cement paste as deduced from sorption-length change and mechanical properties, Materials and Structures 1 (6) (1968) 509–520.
[30] V. Baroghel-Bouny, Experimental investigation of self-desiccation in high-performance materials—Comparison with drying behaviour, in: B. Persson, G. Fagerlund (Eds.), Proceedings of the International Research Seminar Self-Desiccation and Its Importance in Concrete Technology, Lund, Sweden, June 10, 1997, pp. 72–87.
[31] O. Coussy, Mechanics of Porous Continua, John Wiley and Sons, New York, 1995.
[32] O. Coussy, R. Eymard, T. Lassabatère, Constitutive modelling of unsaturated drying deformable materials, J Engineering Mechanics 124 (6) (1998) 658–667.
[33] O. Coussy, T. Lassabatère, Mechanical behaviour of partially saturated porous media—Modelling of drying shrinkage, in: P. Ciarlet (Ed.), Mechanics of Porous Media, Chap. XIV, Balkema, Rotterdam, 1995, pp. 245–264.
[34] J. Carmeliet, Moisture transfer and durability of open reactive porous media, in: Proceedings of 5th Symposium on Building Physics in the Nordic Countries, Espoo, Finland, September 9–10, 1996.
[35] B. Perrin, V. Baroghel-Bouny, L. Chemloul, Methods of determination of the hydric diffusivity of hardened cement pastes, Materials and Structures 31 (1998) 235–241.
[36] T. Lassabatère, Couplages hydro-mécaniques en milieu poreux non saturé avec changement de phase: Application au retrait de dessiccation, Ph.D. thesis, Ecole Nationale des Ponts et Chaussées, 1994.
[37] M. Mainguy, O. Coussy, R. Eymard, Modélisation des Transferts Hydriques Isothermes en Milieu Poreux, Application au Séchage des Matériaux à Base de Ciment, ERLPC, in press.
[38] B.E. Sleep, J.F. Sykes, Compositional simulation of groundwater contamination by organic compounds. 1—Model development and verification, Water Res 29 (6) (1993) 1697–1708.
[39] R. Taylor, R. Krishna, Multicomponent Mass Transfer, John Wiley and Sons, New York, 1993.
[40] D.A. de Vries, A.J. Kruger, On the value of the diffusion coefficient of water vapour in air, in: Proceedings of Colloque Int. du CNRS n° 160: Phénomènes de Transport avec Changement de Phase dans les Milieux Poreux ou Colloidaux, 1966, pp. 61–72.
[41] A. Degiovanni, C. Moyne, Conductivité thermique de matériaux poreux humides: Évaluation théorique et possibilité de mesure, Int J Heat Mass Transfer 30 (11) (1986) 2225–2245.
[42] M.T. van Genuchten, A closed-form equation for predicting the hydraulic conductivity of unsaturated soils, Soil Science Society of America 44 (1993) 892–898.
[43] L. Luckner, M.T. van Genuchten, D.R. Nielsen, A consistent set of parametric models for the two-phase-flow of immiscible fluids in the subsurface, Water Res 25 (10) (1989) 2187–2193.
[44] R.J. Millington, Gas diffusion in porous media, Science 130 (1959) 100–102.
[45] R. Eymard, T. Gallouët, R. Herbin, in: P. Ciarlet, J.L. Lions (Eds.), Handbook of Numerical Analysis. The Finite Volume Method, in press.
[46] E.J. Garboczi, Permeability, diffusivity and microstructural parameters: A critical review, Cem Concr Res 20 (4) (1990) 591–601.